Received May 25, 2020, accepted June 3, 2020, date of publication June 9, 2020, date of current version June 19, 2020.

Digital Object Identifier 10.1109/ACCESS.2020.3000847

A Novel Coupling Structure for Inline Realization of Cross-Coupled Rectangular Waveguide Filters

MUHAMMAD LATIF[1], GIUSEPPE MACCHIARELLA[2], (Fellow, IEEE), AND FAROOQ MUKHTAR[1]

[1]Department of Electrical Engineering, University of Engineering and Technology UET Lahore, Lahore 39161, Pakistan
[2]Department of Electronic, Information and Bioengineering, Politecnico di Milano, 20133 Milano, Italy

Corresponding author: Giuseppe Macchiarella (giuseppe.macchiarella@polimi.it)

ABSTRACT This paper presents a new cross-coupling structure for introducing transmission zeros in waveguide filters with inline configuration. The cross-coupling is realized by an internal bypass metallic loop structure (wire), short-circuited to the filter top plate and passing through the waveguide cavities. Positive and negative cross-couplings are realized by only varying the length of the structure suitably. Full-wave electromagnetic (EM) simulations of the coupling structure are performed for extracting the coupling coefficient sign and value (k). The relationship of the values of k with the coupling structure dimensions is presented graphically. The loading effect of coupling structure on the resonance frequency of the waveguide cavities is also discussed, as well as the possibility of post-manufacturing tunability. The feasibility of the proposed coupling structure is demonstrated by the design of three test filters. Two filters verify the in-line design of a triplet configuration using the proposed coupling wire to introduce a transmission zero below or above the passband. These filters have been also manufactured and measured for an experimental validation of the new structure. The third filter demonstrates the use of the wire loop to create a negative coupling in a cross-coupled configuration. Power handling capability of this configuration has been also thoroughly analyzed by full-wave EM simulation.

INDEX TERMS Cross-coupling, electromagnetic (EM), inline, non-resonating node (NRN), trisection, transmission zeros (TZs), quartet section, waveguide resonators.

I. INTRODUCTION

In recent years, the continuous growth of the frequency channels request has resulted in increasingly stringent requirements on the selectivity of microwave filters used in communication systems. To achieve such a result, the introduction of transmission zeros (TZ) in the frequency characteristic is becoming usual in commercial products. Microwave filters in rectangular waveguide have long been used in the past and still nowadays are employed, especially in space communications equipment [1]. The introduction of TZ in the response of rectangular waveguide filters is typically realized by using folded configuration to allow the cross-couplings implementation (i.e. coupling between non-adjacent resonators) [2]–[4]. On the other hand, the in-line form is the most popular topology of rectangular waveguide filters because it can be easily manufactured and integrated with other subsystems like common manifold multiplexers.

The associate editor coordinating the review of this manuscript and approving it for publication was Feng Lin.

Unfortunately, the in-line topology does not easily allow, basically, the introduction of couplings between non-adjacent resonators. For this reason, various solutions, alternative to the cross-coupled configuration, have appeared in the literature for introducing TZ in the response of in-line rectangular waveguide filters. We can mention, for example, dual-mode cavities filters [5]–[7], evanescent mode filters [8], singlet or doublet implemented inside the waveguide through suitably placed discontinuities [9]–[11], extracted-pole configuration using non-resonating nodes [12]–[14], use of frequency-dependent couplings [15], [16]. All these solutions, however, make unavoidably more difficult the design and, often, more critical and expensive the filter fabrication with respect the basic form of the in-line waveguide filter without transmission zeros (which typically employs inductive irises as coupling structures). To overcome this limitation, we introduce in this work a new coupling structure, allowing the implementation of cross-couplings in rectangular waveguide filters with in-line topology.

This work is licensed under a Creative Commons Attribution 4.0 License. For more information, see https://creativecommons.org/licenses/by/4.0/

The proposed structure consists in a simple metallic wire (with circular or rectangular cross section) inserted inside the waveguide close to the lateral wall, with the terminals connected to the top wall of two non-adjacent cavities (Fig. 1). To the best of authors' knowledge, such a structure has never been proposed in the literature to realize couplings in rectangular waveguides. In [17], a wire terminated with capacitive plates is shown as possible cross-coupling in coaxial cavity filters, but the required isolation from ground (capacitive coupling), the implementation relatively complex (the wire must be inserted inside the lateral wall of the filter housing) and the not good performances regarding the generated spurious resonances make this coupling solution not really attractive.

The coupling structure here introduced allows realizing both positive and negative coupling (simply changing the length). Moreover, the coupling implementation is very simple and filters using this coupling are easy to realize as those with all-pole response. We can also observe that, being the proposed coupling structure ground connected, the transmission of internal heat to an external sink is made easier. The use of this coupling is then attractive for high power applications like output multiplexers for satellite communications.

Various characteristics of the coupling structure have been investigated by performing full-wave EM simulations and post processing. In section II, the coupling structure is introduced and its capability to realize negative and positive coupling is described. The coupling performances are evaluated and presented in section III. Two design examples are given in section IV and measurements on fabricated filters are presented. Tunability of the coupling structure is also described there. Section V shows the use of the novel coupling structure to realize a negative coupling in folded waveguide filters in place of the usual capacitive probe. The power handling of filters employing this coupling structure is also discussed in Section V. Conclusions are drawn in Section VI.

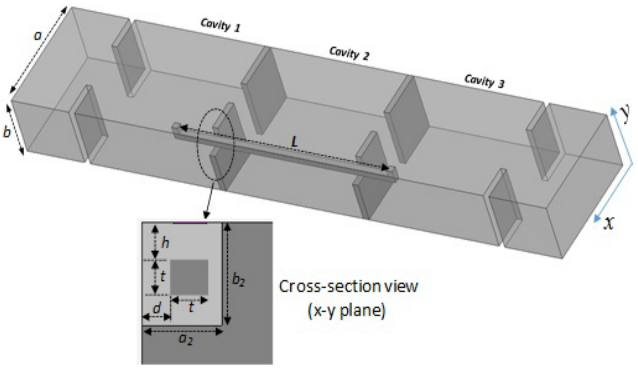

FIGURE 1. Trisection waveguide filter with the proposed coupling structure as cross-coupling between cavity 1 and cavity 3. The relevant geometrical parameters are reported on the drawing.

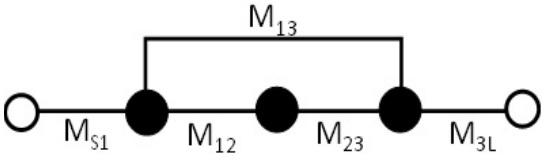

FIGURE 2. Routing scheme of a trisection (3 poles and 1 transmission zeros characteristic function).

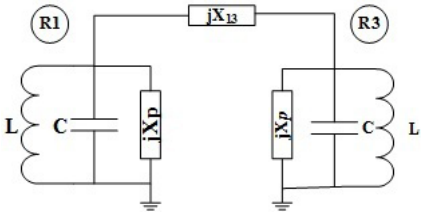

FIGURE 3. Empirical circuit of the proposed cross-coupling structure between resonators R_1 and R_3. X_{13} is the reactance representing the coupling M_{13}, X_p account for the loading effect produced by the loop coupling on the cavity resonators.

II. PROPOSED CROSS-COUPLING STRUCTURE

A waveguide implementation of the trisection topology realizing one TZ is shown in Fig. 1. The cross-coupling between non-adjacent cavities is realized by an internal bypass loop structure formed by a metal strip/wire with opposite ends short-circuited to the top plate of the filter. The strip (or wire) has thickness (or diameter) t. The coupling structure is placed at distance d from the sidewall and height h from the top wall of the filter cavities. The length L of the loop is determined by the position of the short circuits which are symmetrically placed inside the first and last cavities. To allow the strip passing through the cavities, a small rectangular aperture of dimensions (a_2, b_2) is created in the coupling irises. All the relevant parameters of the coupling structure are shown in Fig. 1.

The trisection waveguide filter in Fig. 1 can be schematically represented by the routing scheme in Fig. 2.

There are two types of couplings, mainline positive couplings (M_{s1}, M_{12}, M_{23} and M_{3L}) and one cross-coupling M_{13} (may be positive or negative). For mainline couplings in the direction of propagation, shunt inductance is a good equivalent for the impedance or admittance inverter derived from the normalized coupling matrix. These couplings are realized by irises in the end walls of waveguide cavities as shown in Fig 1. The proposed cross-coupling structure realizing M_{13} is equivalent to sidewall coupling in rectangular waveguide filters, where a coupling window is created in the sidewall at the voltage maximum point of the coupled resonators. From a circuit point of view (Fig. 3), this coupling can be represented by a positive or negative series reactance (X_{13}), connecting two equivalent shunt resonators (representing the coupled waveguide cavities). Note that the shunt reactances X_p are introduced to account for the loading effect of the loop on the equivalent resonators. Note also that the sign of X_{13} is the same of M_{13} parameter [18], [19].

The circuit in Fig. 3 allows evaluating the coupling coefficient k, which is also related to the even (f_{even}) and odd (f_{odd}) mode resonances of the coupled resonators. In fact, it has

[20]:

$$k = \frac{X_{13}}{\omega_0 C} = \frac{f_{even}^2 - f_{odd}^2}{f_{even}^2 + f_{odd}^2} \tag{1}$$

The coupling coefficient concept is the bridge between the equivalent circuit and the physical implementation of coupled resonators structures. Once the value of k has been obtained from the lumped circuit synthesis, we can impose it on the physical coupling structure by means of the full-wave electromagnetic simulation of the structure. In particular, the eigenvalue analysis is employed to get an accurate and fast computation of the resonating modes of the coupled structure, from which k can be evaluated once f_{even} and f_{odd} have been identified among the computed resonance frequencies of the modes. In this regard, we observe that the eigenvalue analysis does not allow to easily evaluate the sign of k. In fact, the eigenmode frequencies are always sorted in ascending order and the proper selection of f_{even} and f_{odd} may require considering the actual field distribution of the computed modes. For this reason, before facing the evaluation of the coupling coefficient for the proposed coupling loop, we will discuss how to identify the sign of k. Despite the method we will present is substantially empirical, it has allowed to correctly identify the values of the loop length L for which k is positive or negative. The method is based on extracting the sign of the equivalent reactance X_{13} by means of an EM simulation. From Fig. 3, we observe that jX_{13} represents the inverse of the admittance parameter Y_{13}. The latter can be evaluated by shorting the shunt resonators, splitting X_{13} into two equal reactances in series and evaluating the impedance Z_{in} in the middle point. From Fig. 4, we get $jX_{13} = 4 \times Z_{in}$. This is replicated in the EM simulator (HFSS has been used) by placing a lumped port at the longitudinal center of the coupling structure between the top plate and the coupling structure as shown in Fig. 4. We assume the input impedance observed at this port equal to the impedance Z_{in} defined in the lumped circuit. The sign of the coupling is then represented by the sign of the imaginary part of Z_{in}, computed by EM simulation. Although it cannot be demonstrated that this method provides the exact value of X_{13}, we have verified by several design examples that it identifies the sign of X_{13} with good accuracy. In the following, all the investigations and analysis of the coupling structure are performed at 10 GHz using WR75 waveguide (a = 19.05 mm, b = 9.525 mm). The assigned loop parameters are t = 1 mm, h = 1 mm, d = [1 mm, 2 mm, 3 mm].

We have removed the resonators from the simulation because they are assumed short-circuited. The loop is inserted in a box whose length is $3\lambda_{g0}$ (with λ_{g0} waveguide wavelength at 10 GHz). The computed Im(Z_{in}) is reported in Fig. 5 for the three assigned values of d, as a function of L normalized to the free space wavelength λ_0. The behavior of Im(Z_{in}) reported in Fig. 5 suggests a possible model for the frequency dependence of X_{13}. In fact, the loop can be represented by two short-circuited transmission lines connected in parallel at the point where the lumped port is placed,

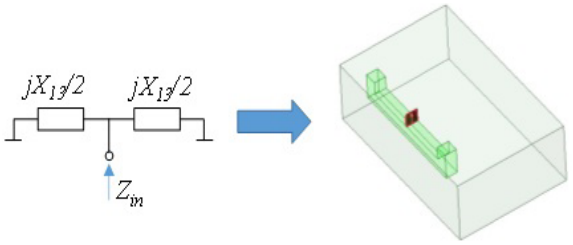

FIGURE 4. EM model for Z_{in} calculation. A lumped port is placed at the mid-point of the loop.

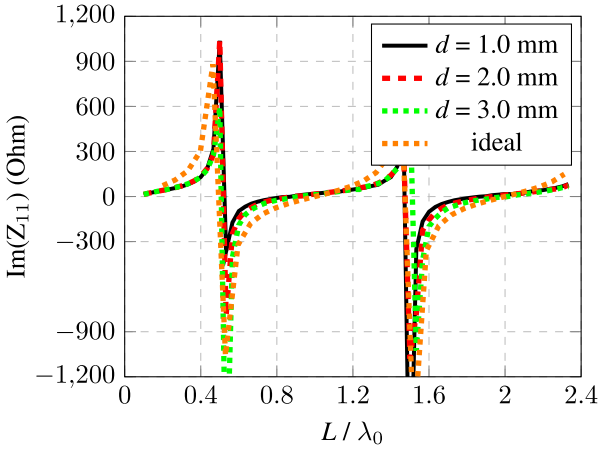

FIGURE 5. Computed Im(Z_{11}) vs. L / λ_0 ($w = t = h$ = 1.0 mm).

providing the following expression for the impedance Z_{in} [21].

$$Z_{in} = j\frac{Z_c}{2} tan(\pi \frac{L}{\lambda_0}) \tag{2}$$

With a suitable choice of the characteristic impedance Z_c, the computed Z_{in} by full-wave simulation can be well reproduced by this model. This is shown in Fig. 5 where the curve computed with the model is reported (dashed orange curve, Z_c = 100 Ohm).

Note that the reason we have assumed a TEM transmission line model is that the physical structure of the loop can be assimilated to a thick microstrip in air (t is the strip thickness and h is gap between the strip and the ground plane, represented by the top wall of the enclosure). Assuming the proposed model for Z_{in}, we observe that positive coupling can be achieved for $n\lambda_0 < L < (2n+1)\lambda_0/2$, where $n \geq 0$ is an integer. The condition for negative coupling is $(2m-1)\lambda_0/2 < L < m\lambda_0$ where $m > 0$ is a positive integer. For the assigned coupling coefficient sign, the length L of the loop is chosen and is placed in longitudinal symmetry between the coupled resonators. Following the procedure in section III, the value of the coupling coefficient k can be finally determined. The model of the loop above introduced suggests that this structure can also be used as an embedded TEM resonator in the waveguide structure. Advanced filtering functions may be realized using this embedded resonator, but further research

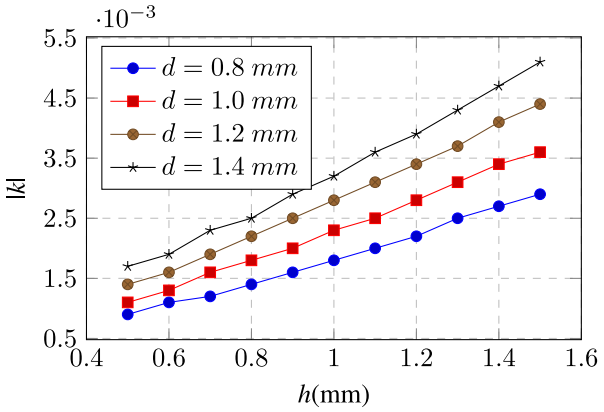

FIGURE 6. Relation between the coupling coefficient k and height h for negative M_{13} coupling. (t = 1.0 mm).

is required for validating this concept (in particular the effects due to the relatively low unloaded Q of this resonator).

III. CROSS-COUPLING STRUCTURE ANALYSIS

The net coupling between resonators can be inductive or capacitive. Once the nature of the coupling is determined using method described in section II, the coupling coefficient k can be calculated by using the eigenmodes solver of an EM simulator [20].

$$|k| = |\frac{f_1^2 - f_2^2}{f_1^2 + f_2^2}| \tag{3}$$

The frequencies f_1 and f_2 are the eigenmode frequencies of mode 1 and mode 2 in the eigenmode analysis of the waveguide structure given in the Fig.1 (with all couplings between adjacent cavities set to zero). Initially, all three resonators are designed to resonate on TE_{101} mode at 10 GHz (physical length equal to 24.285 mm in WR75 waveguide). As the coupling under consideration is M_{13} resonator 2 must be strongly detuned by means of a tuning screw. The effect of coupling structure dimensions on the coupling coefficient k has been thoroughly analyzed both for negative and positive couplings. For negative coupling, the relation between k and height h is shown in Fig. 6. By changing h from 0.5 mm to 1.5 mm, k can be varied from 0.0009 to 0.0056. These values are large enough to realize narrow to moderate bandwidth filters. From Fig. 6, it is evident that the coupling increases with d and h. In fact, when these parameters increase, the loop is moved towards higher E field region.

This phenomenon is evident from the electric field plot inside the coupled resonators shown in Fig. 7. Electric field is confined between coupling structure and sidewalls in resonator 2. Therefore coupling between resonators 1 and 3 is strong and coupling between resonators 1 and 2 is negligibly small.

Rigorous EM simulations were performed to observe the relation between k and cross-section (width w and thickness t) of the coupling structure for fixed h and d. Simulation results

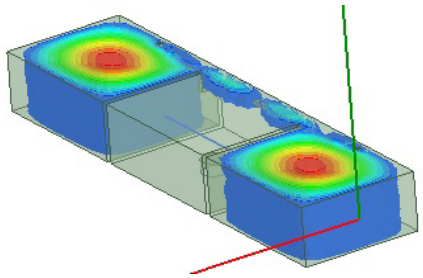

FIGURE 7. Electric field plot inside the coupled resonators structure. (Field in Resonators R_1 and R_3 is strong.)

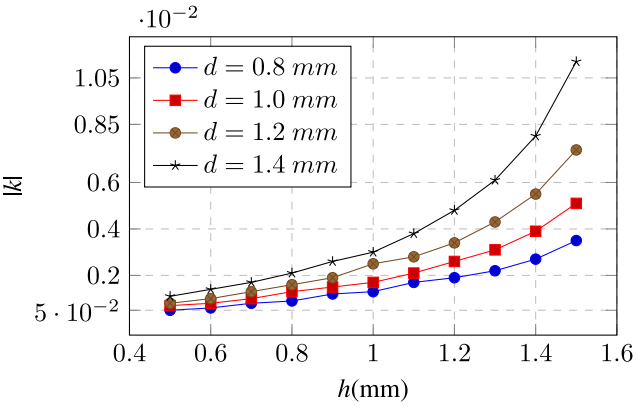

FIGURE 8. Relation between the coupling coefficient k and height h for positive M_{13} coupling. (t = 1.0 mm).

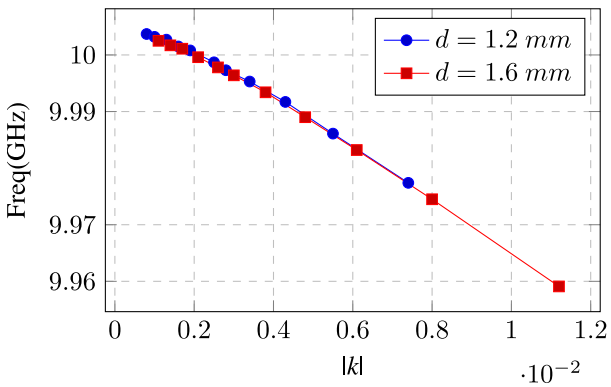

FIGURE 9. Relation between the coupling coefficient k and average resonance frequency of coupled resonators for positive M_{13} coupling.

were similar to the data presented in Fig. 6 and are not presented to avoid repetition.

The coupling structure for positive M_{13} is structurally similar to its counterpart negative cross-coupling structure. Simulation results show that k can be varied from 0.0005 to 0.012. The comparison of simulation results shows that rate of rising of k for positive coupling is higher compared to negative coupling as shown in Fig. 8.

The loading effect of the coupling structure on the coupled resonators 1 and 3 can be related to the shift in the resonance frequency of uncoupled resonators determined by eigenmode analysis. Fig. 9 shows the relation of k and average reso-

nance frequency of the coupled resonators (resonator 1 and resonator 3). Due to loading effect of the coupling structure, the frequency is lower than the resonance frequency of uncoupled resonators (10 GHz). The physical length of resonators 1 and 3 must be slightly decreased to compensate the loading effect. Resonator 2 is bypassed by the coupling structure, therefore a loading effect on resonator 2 was also observed. The length of the resonator 2 must be slightly increased to compensate the loading effect of the coupling structure. EM simulations were also performed to analyze the loading effect of negative M_{13} couplings. In this case, the loading effect can be compensated by slightly increasing the length of coupled resonators.

IV. FILTER DESIGN EXAMPLES

Two filter design examples are presented to validate (also experimentally) the proposed concept. Third-order asymmetric filter characteristic functions (3-1) are realized for both designs, centered at $f_0 = 10$ GHz, equiripple bandwidth BW = 40 MHz and return loss level of 22 dB. Filter1 has a normalized TZ at −j3 (attenuation pole at 9.940 GHz, on the lower side of the passband) whereas Filter2 has a normalized TZ at +j3 (attenuation pole at 10.06 GHz, on the upper side of the passband). The attenuation lobe level is around 35 dB for both cases. Interface waveguide for both designs is WR75, having internal width $a = 19.05$ mm and height $b = 9.525$ mm. The normalized coupling matrices (CM) are M_1 and M_2 for Filter1 and Filter2 respectively. R_1 and R_2 are normalized input and output terminations [22].

$$M_1 = \begin{pmatrix} -0.1073 & 1.0426 & -0.4159 \\ 1.0426 & 0.3863 & 1.0426 \\ -0.4159 & 1.0426 & -0.1073 \end{pmatrix} \quad (4)$$

$$R_1 = R_2 = 1.2944 \quad (5)$$

$$M_2 = \begin{pmatrix} 0.1073 & 1.0426 & 0.4159 \\ 1.0426 & -0.3863 & 1.0426 \\ 0.4159 & 1.0426 & 0.1073 \end{pmatrix} \quad (6)$$

The full-wave EM dimensioning starts by designing irises for mainline sequential couplings. For irises with symmetric structure on both sides, couplings can be transformed to measurable scattering parameters like $|S_{21}|$ and $\angle S_{21}$ [23], [24]. These parameters can be used to calculate the iris dimensions for input/output coupling, inter-resonator couplings and loading effect of these couplings. The loading effect can be considered as an FIR (Frequency Invariant Reactance) and will be absorbed in the corresponding resonators. The aperture for passing through the cross-coupling structure can be considered as part of mainline couplings and can be designed accordingly. Mainline couplings' value for both filters are the same; therefore, iris widths for both filters are the same. Fig.10a shows the iris parameters for mainline couplings (all irises are of 1.0 mm thickness). Waveguide filter structure, relevant parameters of cavity resonators and interface waveguide dimensions are shown in Fig.10.

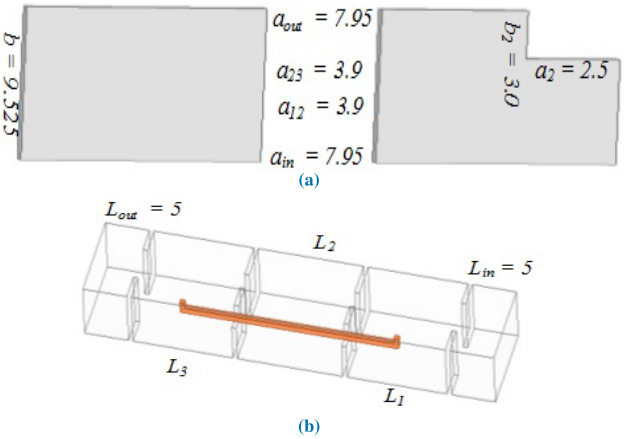

FIGURE 10. (a) Iris parameters for both design examples, input/output iris widths (a_{in}, a_{out}), sequential coupling iris widths (a_{12}, a_{23}). (b) Waveguide filter structure for trisection realizing M_{13} using the proposed coupling structure, Ls are lengths of input/output waveguides and resonator cavities (All length dimensions are in mm).

TABLE 1. Prototype Filters' dimensions (mm).

S.No.	Parameter	Filter1	Filter2
1	Length of resonators 1 and 3	22.69	22.618
2	Length of resonator 2	23.95	23.88
3	Thickness of coupling loop (t)	1	1
4	Height of coupling loop (h)	0.75	1.05
5	Coupling loop offset from sidewall (d)	1	1
6	Length of coupling loop (L)	47.64	35.64
7	Iris aperture (a_{in} , a_{out})	7.95	7.95
8	Iris aperture (a_{12} , a_{23})	3.9	3.9
9	Aperture (a_2)	2.5	2.5
10	Aperture (b_2)	3	3

For M_{13} of the first example

$$k_{13} = \frac{M_{13} \times BW}{f_0} = -1.66 \times 10^{-3} \quad (7)$$

From Fig. 6 ($d = 1$ mm), we can obtain the h value producing the required k_{13} ($h = 0.75$ mm). Proceeding similarly for the second filter we obtained $h = 1.05$ mm. For both filters, the length of the cavities has been corrected to take into account the loading effect of the coupling wire. The dimensions of Filter1 and Filter2 are given in Table 1. The common dimensions for both designs are shown in Fig. 10.

All the dimensions of both filters are the same except cavity lengths and coupling loop parameters. The coupling loop can be integrated with the filter structure through a couple of holes in the top plate. The prototype filter was manufactured using CNC machining. The filter top lid with the connected wire coupling is shown in Fig. 11a, while the internal structure of the filter is reported in Fig. 11b (overall dimensions 38.1 mm × 38.1 mm × 94.0 mm). It can be noticed that the filter structure is as easy to manufacture as the classical all-pole filter with inductive irises. Moreover, a fine tuning of the TZ frequency is possible in post-production, as will be discussed in the following.

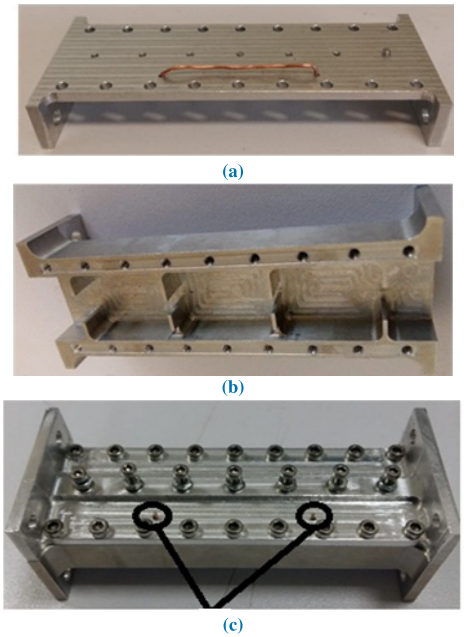

FIGURE 11. (a) Top lid of the filter with wire forming the M_{13} coupling loop, (b) Internal structure of the filter, (c) Assembled structure of the filter.

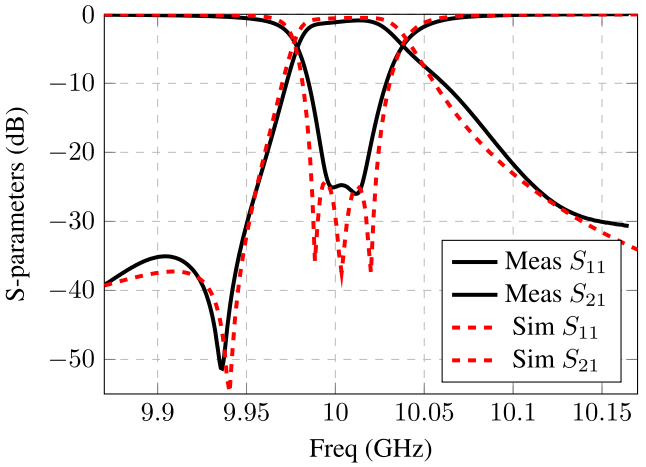

FIGURE 12. Comparison of measured and EM simulation results of the filter having TZ below the passband (solid lines are measured results and dotted lines are EM results.)

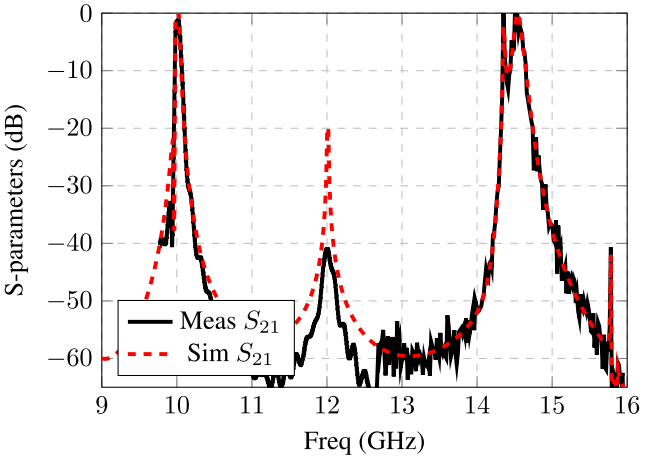

FIGURE 13. Comparison of broad band measured and EM simulation results of the filter having TZ below passband (solid lines are measured results and dotted lines are EM simulation results.)

EM simulation and measured S-parameters of the filter having TZ below the passband are reported in Fig. 12. The position of TZ in simulation is at 9.940 GHz whereas in measurement TZ is at 9.935 GHz. This shift in the TZs is due to a slight increase in bandwidth (measured equiripple BW = 43 MHz and simulated BW = 40 MHz). The measured insertion loss at f_0 is 0.8 dB. The loss is higher than expectation due to low cost prototype (no silver plating) The simulated and measured S_{11} is less than -20 dB within the entire passband. Note that the slight ripple observed in the out-of-band response in Fig. 12 is likely due to a poor grounding of the coupling wire with the filter top plate. In fact the wire terminals are not bonded or welded with the lid but only forced in small holes. Consequently, not good contact may have been obtained. Wideband performance of the filter is presented in Fig. 13. A spurious resonance can be observed at relatively large distance from the passband (2 GHz). Note that the spike level is low, because the coupling from input to output through the coupling loop is very weak and waveguide resonators are decoupled at this frequency. As described in the previous section, the loop length selection allows flexibility, therefore spike position can be relatively controlled. Spurious passband at 14.68 GHz is due to TE_{102} mode resonance of waveguide resonators at this frequency. In Section V we will show that, using a compact loop, the spike can be moved above the TE_{102} mode resonance of the waveguide resonators.

EM simulation and measured S-parameters of the filter having TZ above the passband are reported in Fig. 14. The position of TZ in simulation and measurements are 10.06 GHz and 10.082 GHz respectively. This displacement is owing to the widening of the bandwidth (measured equiripple BW = 50 MHz and simulated BW = 40 MHz). The increase in bandwidth of both filters may be due to the manufacturing tolerances of the coupling irises. The presence of the coupling wire could also increase the coupling produced by the irises. The simulated and measured S_{11} is less than -18 dB within the passband. The measured insertion loss at f_0 is 0.7 dB. The loss is higher than expectation due to low cost prototype (no silver plating, wire loop not bonded or welded).

Fig. 15 shows the wideband performance of the filter realizing TZ above the passband (only EM simulations are reported). In this case, TZ is closer to the passband, but the distance (1 GHz) remains very large (compared to the bandwidth)

It has been remarked that the novel coupling structure allows the realization of rectangular waveguide filters with in-line topology and TZ in the frequency response. It is then interesting to compare a filter that uses the novel coupling with a classical reference filter having the same features.

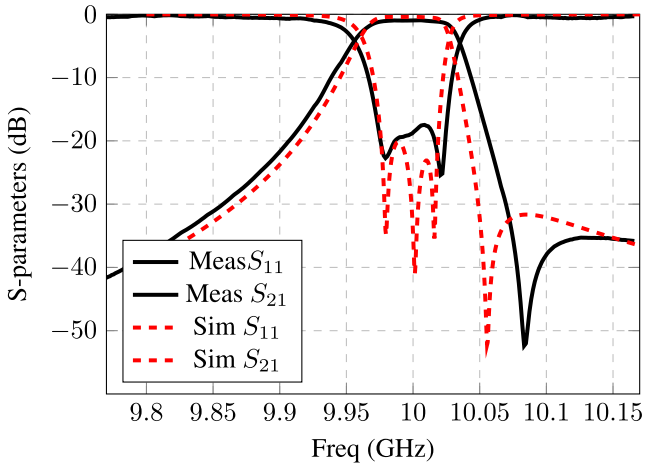

FIGURE 14. Comparison of measured and EM simulation results of the filter having TZ above the passband (solid lines are measured results and dotted lines are EM simulation results.)

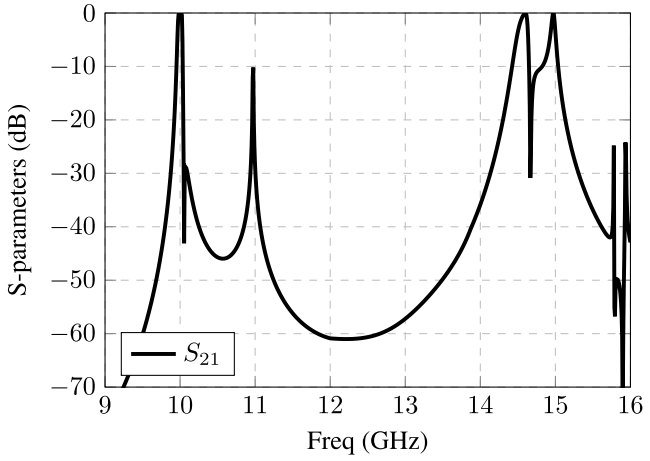

FIGURE 15. Broad band EM simulation results of the filter having TZ above passband.

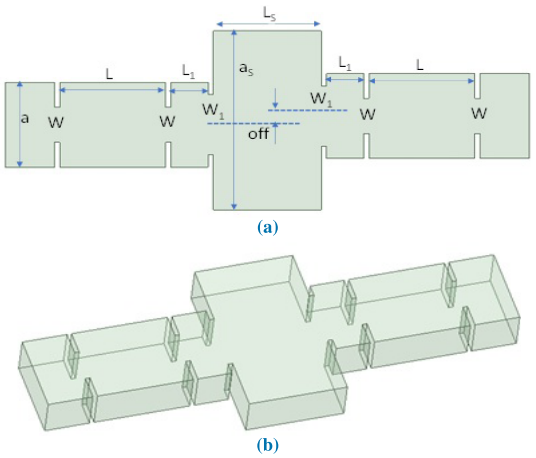

FIGURE 16. (a) top view of extracted-pole waveguide filter with Input/output waveguides (and resonators): a = 19.05, b = 9.525, W = 7.8941, W_1 = 13.5911, L = 21.39, L_1 = 7.57, a_s = 40.2, L_s = 21.8554, t = 1, off = 0.966 (All dimensions in mm) (b) 3D view of the extracted pole filter.

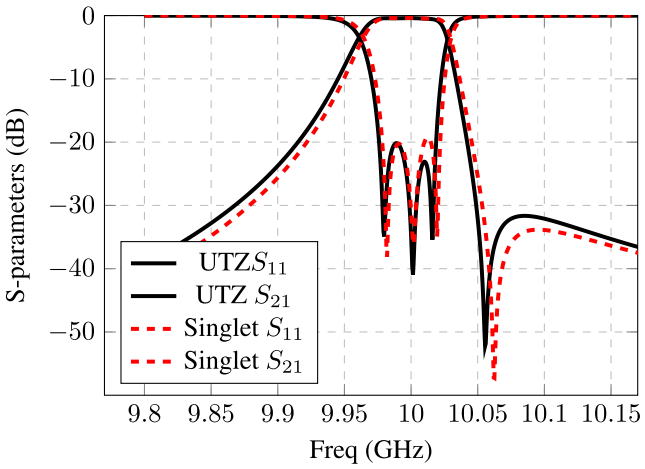

FIGURE 17. Comparison of EM simulation results of trisection realized using internal loop structure and extracted pole implementation of trisection (solid lines are for loop based trisection and extracted pole based trisection results are dotted lines.)

We have selected to this purpose an extracted-pole filter, being an in-line topology widely used in the practice. The reference filter adopts singlets blocks for the TZ extraction [25] and has been designed with the same requirements of the test tri-section filter with upper TZ. The filter structure and its parameter values are shown in Fig. 16. Both filters have been simulated including losses in the conductors (silver conductivity is assumed). EM simulation results of both filters are plotted in Fig. 17. Filter with an internal loop has mid-band insertion loss of 0.40 dB whereas the extracted pole filter has insertion loss of 0.38 dB. The advantage of the novel solution is the filter overall size (93.12 mm × 19.05 mm × 9.525 mm), much smaller of the extracted-pole solution (105.8 mm × 40.2 mm × 9.525 mm). It must be remarked that the same losses are obtained with both the solutions but the one employing the loop coupling allows a noticeable reduction of both the filter volume and footprint.

The feasibility of post-manufacturing tuning has been investigated by means of EM simulations. Tuning allows to refine the position of TZ, whose placement may be affected by fabrication tolerances. To this purpose, a tuning screw inserted in close vicinity of the coupling structure can be used as shown in Fig. 18a. The results of EM simulations (Fig. 18b) show that a very accurate positioning of TZ can be obtained in this way. For example, a tuning screw of 2.0 mm diameter, initially penetrated 0.5 mm can move TZ 8 MHz towards the passband by further penetration of 1.2 mm.

Finally, we remark the capability of the proposed structure to place transmission zeros very close to the passband. For example, considering the filter with the zero below the passband, we can move up the zero to 9.975 GHz. Fig. 6 shows, in fact, the feasibility of the required cross-coupling (equal to −0.0047).

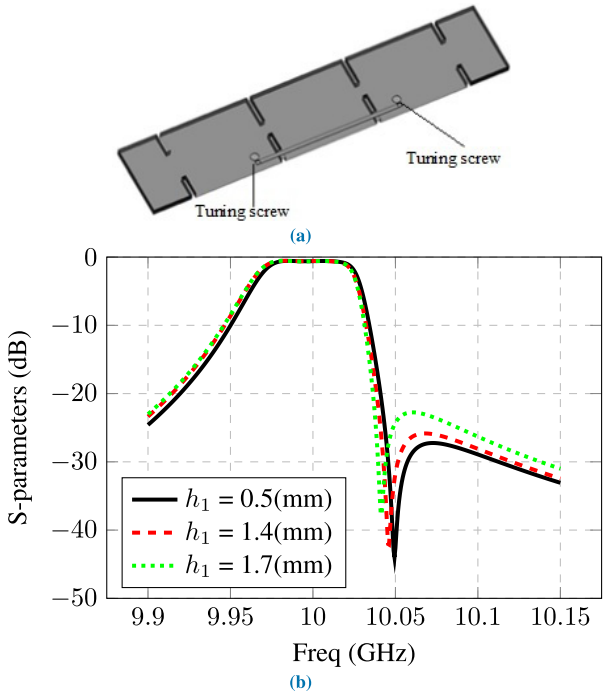

FIGURE 18. (a) EM model of filter for tuning capability analysis, only top view is shared to show the location of tuning screws and coupling loop. (b) Relation between tuning screw penetration h_1 and TZ, with increase in M_{13} coupling, TZ is approaching to passband.

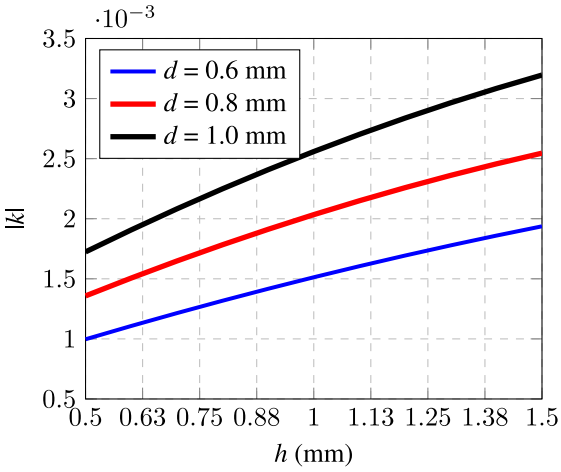

FIGURE 19. Relation between the coupling coefficient k and height h for $L = 17.739$ mm and $t = 1.0$ mm.

V. ANOTHER APPLICATION OF THE NOVEL COUPLING LOOP

Although the main goal of the proposed coupling loop is the realization of in-line waveguide filters with transmission zeros, it can be also advantageously adopted in classical cross-coupled configurations requiring negative couplings. In these cases, a capacitive probe is often adopted, which however suffers from some drawbacks due to the isolation requirement from the filter body. It can be mentioned, for instance, the reduced power handling capability and the increased fabrication complexity. These drawbacks can be overcome by using the novel coupling loop, as illustrated in the design example reported in the following.

A. DESIGN OF A QUARTET SECTION FILTER

The quartet section is a basic building block of many advanced filtering structures. Although, strictly speaking, this topology is not in-line, the use of the novel loop structure makes easier and cheaper the waveguide implementation of the quartet, compared to other possible solutions.

A design example (Filter3) is then presented to illustrate the application of the new loop coupling in the quartet configuration. As known, with this 4-pole topology we can introduce two symmetric TZ by means of a single cross-coupling between resonators 1 and 4. The following requirements are assumed for Filter3: Center frequency $f_0 = 10$ GHz, bandwidth BW = 40 MHz, Return Loss RL = 22 dB, normalized transmission zeros $\Omega_z = \pm j1.7$ (which correspond to de-normalized frequencies 9.966 GHz and 10.034 GHz). The synthesis of the coupling matrix produces the following result:

$$M_3 = \begin{pmatrix} 0 & 0.8800 & 0 & -0.2938 \\ 0.8800 & 0 & 0.8331 & 0 \\ 0 & 0.8331 & 0 & 0.8800 \\ -0.2938 & 0 & 0.8800 & 0 \end{pmatrix} \quad (8)$$

$$R_1 = R_2 = 1.1297 \quad (9)$$

The design methodology presented in Section III is applied to calculate the dimensions of the filter. Also in this case inductive irises are used for the mainline couplings, although the couplings 1-2 and 3-4 are implemented in the side wall instead of the end wall.

Coupling sign and dimensions of the coupling loop can be calculated using the analysis procedure described in sections II and III. However, since there is no cavity to by-pass, the loop is much shorter than in the case of the trisection, with the beneficial effect of pushing spurious resonance to a much higher frequency.

For the dimensioning of the loop, we have first assigned the length $L = 17.739$ mm, chosen in the range $\lambda_0/2 < L < \lambda_0$ to get a negative value for k_{14}. Then, a chart similar to the one in Fig. 6 has been computed, reporting k as a function of the parameter h (height of the loop), for different values of the separation d from the sidewall (Fig. 19).

From Fig. 19, assigning $d = 0.6$ mm and $h = 0.7$ mm, we get the required value of $k_{14} = (\mathrm{BW}/f_0) \times M_{14} = -0.00117$. The other relevant dimensions of the designed quartet filter are reported in Table 2, while the filter structure is shown in Fig. 20.

Full-wave EM simulation results of the filter structure, reported in Fig. 21, show a close matching to theoretical design requirements. Insertion loss at the center of the filter passband is 0.54 dB, corresponding to an average unloaded Q of the resonators equal to 7300.

TABLE 2. Quartet section based filter's dimensions (mm).

S.No.	Parameter	Filter3
1	Length of resonators 1 and 4	22.74
2	Length of resonator 2 and 3	23.79
3	Thickness of coupling loop (t)	1
4	Height of coupling loop (h)	0.7
5	Coupling loop offset from sidewall (d)	0.6
6	Length of the coupling loop (L)	17.74
7	Iris aperture (a_{in} , a_{out})	7.83
8	Iris aperture (a_{12} , a_{34})	3.22
9	Iris aperture (a_{23})	3.64
10	Aperture (a_2)	3
11	Aperture (b_2)	3

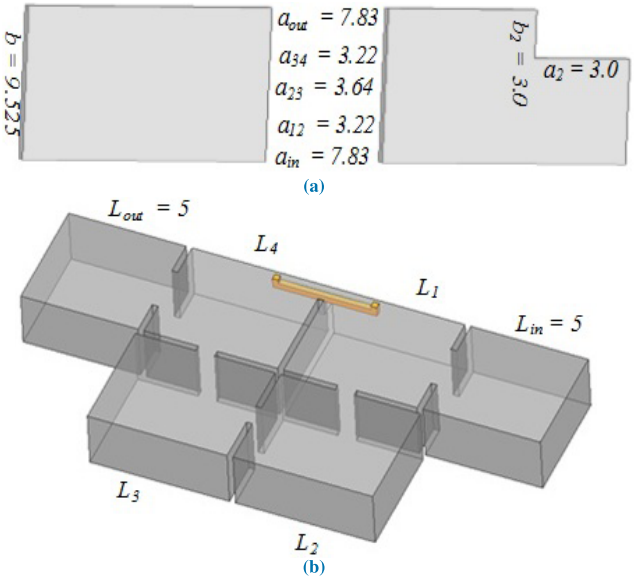

FIGURE 20. (a) Iris parameters for quartet section based filter, input/output iris widths (a_{in}, a_{out}), sequential coupling iris widths (a_{12}, a_{23}). (b) Waveguide filter structure for trisection realizing M_{14} using the proposed coupling structure, L_k are lengths of input/output waveguides and resonator cavities (All length dimensions are in mm).

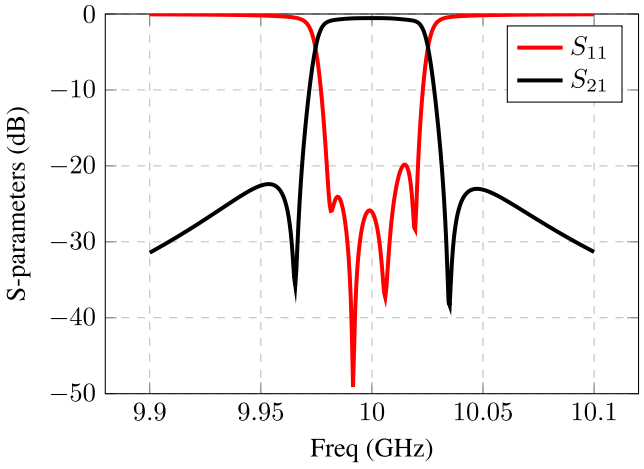

FIGURE 21. Narrow band EM Simulation results of 4th order filter (4-2).

Broadband simulation results of the filter are shown in Fig. 22. We can observe that the loop resonance has moved

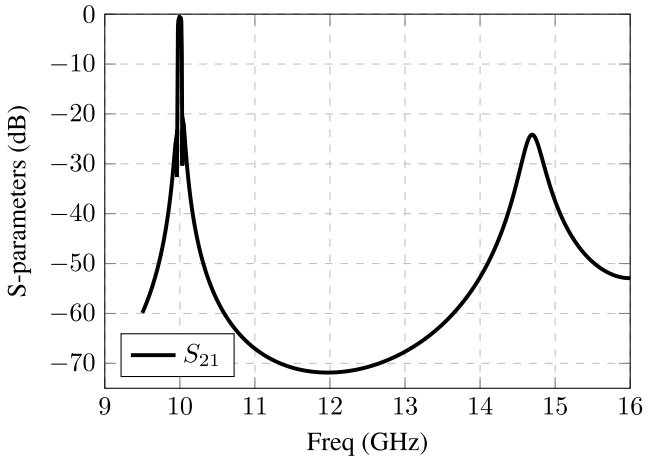

FIGURE 22. Broad band EM Simulation results of 4th order filter (4-2).

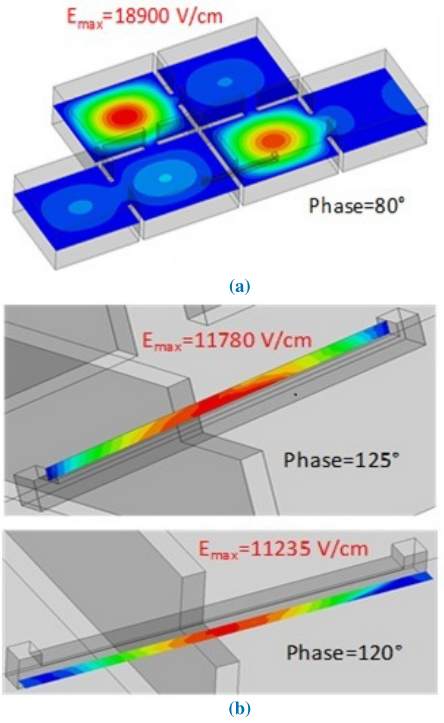

FIGURE 23. (a) Electric field plot inside the filter structure. (b) Electric field plot in close vicinity of the coupling loop.

above the TE_{102} mode resonance. The low level of first spurious band at 14.7 GHz is due to weak coupling of side irises to TE_{102} resonant mode.

B. POWER HANDLING CAPABILITY OF THE LOOP COUPLING

As previously mentioned, the use of the proposed coupling structure is particularly convenient in high power filters. Therefore, we have investigated the possible limitations on power handling introduced by the coupling loop. To this purpose, the electric field distribution inside the quartet filter body (Fig. 20) has been computed by means of a full-wave

simulator (HFSS). We know from the filters theory that the RF voltage across the equivalent resonators ($V_{RF,k}$) is frequency dependent and varies from resonator to resonator [26]. For the considered filter, the RF voltage on resonator 2 ($V_{RF,2}$) is larger than that on the other resonators, at all frequencies in the passband (assuming the exciting signal tone applied at port 1). Although the maximum of $V_{RF,2}$ is close to the passband edges, it must be considered that most of the signal energy is concentrated around the center of the passband (f_0), so limitations to the filter power handling due to possible breakdown phenomena have been investigated at f_0. We have first verified that the maximum E-field is found on cavity 2. Fig. 23a shows the computed E-field with 5 KW input power (single sinusoidal tone applied at port 1). Note that the instantaneous peak value of the E field depends on the phase of the input tone. In the considered case, the maximum of E (E_{max}) has been found on the second cavity (as expected), and it results $E_{max} = 19$ KV/cm (below the theoretical limit for the air breakdown, equal to 22.8 KV/cm). We have then evaluated the E-field in critical areas around the coupling loop, where the field is presumably relatively large. In Fig. 23b the result of the simulations are shown. The peak value in the first area is $E_{max,1} = 11.235$ KV/cm and $E_{max,2} = 11.78$ KV/cm in the second area (note that these results are obtained with different values of the exciting tone phase). Comparing $E_{max,1}$ and $E_{max,2}$ with E_{max}, we note that the peak values of the E field near the loop are well below the maximum at the cavity center. We conclude observing that power-handling capability of microwave filters depends on many other environmental factors and their cumulative effect is difficult to estimate accurately through basic EM simulations. Nevertheless, the computed results show that, very likely, the novel coupling loop does not play a limiting role for the maximum allowed power.

C. REALIZABLE BANDWIDTH AND PERFORMANCE COMPARISON

As a last observation, we want to remark the capability of the proposed coupling structure to realize the coupling coefficients required in moderate/large bandwidth filters. Although typical applications of waveguide filters call for a normalized bandwidth of a few percent, in some special cases a bandwidth as large as 10% may be required. Design of such filters requires extensive use of numerical optimization to account for the strong frequency dispersion of the waveguides. A limiting factor may also arise from the high value of the required coupling coefficients, especially those referring to the cross-couplings. This, however, is not the case with the proposed new coupling loop. In fact, we have evaluated the values of the coupling k_{14} used in the quartet example above reported by modifying some dimensions in order to increase the realizable values. In particular, we have assigned $L = 20.336$ mm, $a_2 = 5$ mm, $b_2 = 4$ mm. Fig. 24 shows the computed k_{14} vs. h, for three values of d (2.5 mm, 3 mm, 3.5 mm).

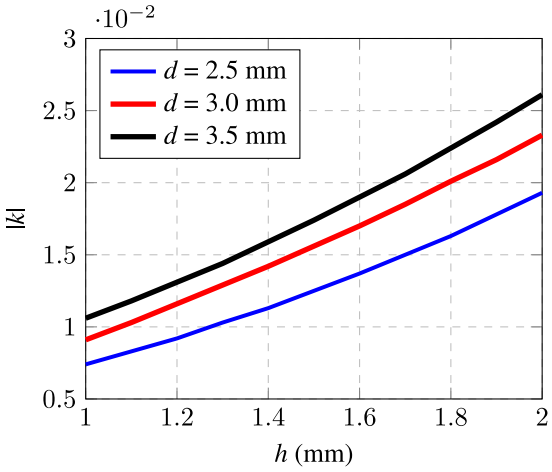

FIGURE 24. Coupling coefficient k_{14} in the quartet configuration of Fig. 20 as function of the height h, for three values of d. ($L = 20.336$ mm, $t = 1.0$ mm, $a_2 = 5$ mm, $b_2 = 4$ mm).

TABLE 3. Performance comparison of proposed coupling (Loop) with conventional coupling (Probe).

Parameter	proposed coupling (Loop)	conventional coupling (Probe)
Compactness	High	Moderate
Design Complexity	Low	Moderate
Power handling Capability	High	Low
Spurious Response	Fair	Good
Bandwidth	Moderate	Narrow
Tunabilty	Low	Moderate

Observing the computed results, the large realizable values of k_{14} can be appreciated. As a reference, a quartet filter with 8% normalized bandwidth at 10 GHz, with two normalized TZs at $\Omega_z = \pm$j1.7, requires $k_{14} = -0.0236$, which can be implemented with the loop coupling considered in Fig. 24 by assigning $d = 3.5$ mm and $h = 1.87$ mm. Note that such a large coupling coefficient is hard to be achieved with the conventional capacitive probe usually adopted to implement a negative cross-coupling in waveguide filters. Table 3 shows the performance comparison of the proposed loop coupling with a conventional probe.

VI. CONCLUSION

A new cross-coupling loop structure for true inline realization of cross-coupled waveguide filters has been proposed and discussed in this paper. Rigorous EM simulation results have been presented to demonstrate that the new coupling structure has the ability to realize positive and negative coupling values by adjusting its length. In fact, although the proposed coupling is intrinsically magnetic, the sign can be reversed because the central portion of the coupling acts like a transmission line, whose length impacts on the coupling sign. The desired level is achieved by adjusting the height from top plate of filter, cross-section and distance of the coupling structure from the sidewall of the filter. Two prototype filters with triplet topology have been fabricated, one having the

TZ below the passband and the other with the TZ above the passband. Measured results validate the coupling structure's capability of realizing cross-coupling and generating TZs.

A quartet section based filter design example is also presented to show that the proposed loop coupling structure can be a potential candidate for the realization of advanced filtering structures having a wide spurious free band. By analysis of E-field inside the filter structure, it is also demonstrated that the novel coupling structure is suitable for realizing high power filters. It is also predicted that the coupling structure can realize an embedded TEM mode resonator inside the waveguide structure, which may lead towards the realization of advanced filter functions in a compact structure.

ACKNOWLEDGMENT

Author would like to thank Dr. I.E. Rana for mentoring throughout the studies and technical carrier. Thanks to Dr. M. R. Suddle (SI,NI), M. Y. Khan, Dr. M. A. Mughal and N. Faisal for their continuous support. Thanks to Dr. G. Ahmad for his continuous support in paper writing. Special thanks to A.-U. Salfi, Z. Ali, R. Iqbal, A. Rafiq, M. Farooq, A. Rehman, and M. Shafi for fabrication, assembling and tuning of the filter structure.

REFERENCES

[1] R. J. Cameron, C. M. Kudsia, and R. R. Mansour, "Radio frequency (RF) filter networks for wireless communications—The system perspective," in *Microwave Filters for Communication Systems: Fundamentals, Design, and Applications*. Hoboken, NJ, USA: Wiley, 2018, pp. 1–74.

[2] R. J. Cameron, "Advanced coupling matrix synthesis techniques for microwave filters," *IEEE Trans. Microw. Theory Techn.*, vol. 51, no. 1, pp. 1–10, Jan. 2003.

[3] C. Carceller, P. Soto, V. Boria, M. Guglielmi, and D. Raboso, "New folded configuration of rectangular waveguide filters with asymmetrical transmission zeros," in *Proc. 44th Eur. Microw. Conf.*, Rome, Italy, Oct. 2014, pp. 183–186.

[4] S. Cogollos, P. Soto, M. Brumos, V. E. Boria, and M. Guglielmi, "Novel rectangular waveguide structures for advanced filter characteristics," in *IEEE MTT-S Int. Microw. Symp. Dig.*, Tampa, FL, USA, Jun. 2014, pp. 1–4.

[5] P. Savi, D. Trinchero, R. Tascone, and R. Orta, "A new approach to the design of dual-mode rectangular waveguide filters with distributed coupling," *IEEE Trans. Microw. Theory Techn.*, vol. 45, no. 2, pp. 221–228, Feb. 1997.

[6] M. Guglielmi, O. Roquebrun, P. Jarry, E. Kerherve, M. Capurso, and M. Piloni, "Low-cost dual-mode asymmetric filters in rectangular waveguide," *IEEE MTT-S Int. Microw. Symp. Dig.*, Phoenix, AZ, USA, vol. 3, May 2001, pp. 1787–1790.

[7] J.-F. Liang, X.-P. Liang, K. A. Zaki, and A. E. Atia, "Dual-mode dielectric or air-filled rectangular waveguide filters," *IEEE Trans. Microw. Theory Techn.*, vol. 42, no. 7, pp. 1330–1336, Jul. 1994.

[8] H.-C. Chang and K. A. Zaki, "Evanescent-mode coupling of dual-mode rectangular waveguide filters," *IEEE Trans. Microw. Theory Techn.*, vol. 39, no. 8, pp. 1307–1312, Aug. 1991.

[9] C. Tomassoni and R. Sorrentino, "A new class of pseudoelliptic waveguide filters using dual-post resonators," *IEEE Trans. Microw. Theory Techn.*, vol. 61, no. 6, pp. 2332–2339, Jun. 2013.

[10] S. Bastioli, L. Marcaccioli, and R. Sorrentino, "Waveguide pseudoelliptic filters using slant and transverse rectangular ridge resonators," *IEEE Trans. Microw. Theory Techn.*, vol. 56, no. 12, pp. 3129–3136, Dec. 2008.

[11] S. Amari, "Direct synthesis of cascaded singlets and triplets by non-resonating node suppression," in *IEEE MTT-S Int. Microw. Symp. Dig.*, San Francisco, CA, USA, Jun. 2006, pp. 123–126.

[12] Y. Yang, M. Yu, and Q. Wu, "Advanced synthesis technique for extracted pole and NRN filters," in *IEEE MTT-S Int. Microw. Symp. Dig.*, San Francisco, CA, USA, May 2016, pp. 1–4.

[13] M. Fahmi, J. A. Ruiz-Cruz, R. R. Mansour, and K. A. Zaki, "Compact ridge waveguide filters using non-resonating nodes," in *IEEE MTT-S Int. Microw. Symp. Dig.*, Boston, MA, USA, Jun. 2009, pp. 1337–1340.

[14] G. Macchiarella and M. Politi, "Use of generalized coupling coefficients in the design of extracted-poles waveguide filters with non-resonating nodes," in *IEEE MTT-S Int. Microw. Symp. Dig.*, Boston, MA, USA, Jun. 2009, pp. 1341–1344.

[15] L. Szydlowski, A. Lamecki, and M. Mrozowski, "Coupled-resonator waveguide filter in quadruplet topology with frequency-dependent coupling—A design based on coupling matrix," *IEEE Microw. Wireless Compon. Lett.*, vol. 22, no. 11, pp. 553–555, Nov. 2012.

[16] G. Macchiarella, G. Gentili, and L. Accatino, "Stopband singlet: A novel structure implementing resonating couplings," *IEEE Microw. Wireless Compon. Lett.*, vol. 30, no. 5, pp. 473–476, May 2020.

[17] Y. Wang and M. Yu, "True inline cross-coupled coaxial cavity filters," *IEEE Trans. Microw. Theory Techn.*, vol. 57, no. 12, pp. 2958–2965, Dec. 2009.

[18] S. Amari and U. Rosenberg, "Synthesis and design of novel in-line filters with one or two real transmission zeros," *IEEE Trans. Microw. Theory Techn.*, vol. 52, no. 5, pp. 1464–1478, May 2004.

[19] R. J. Cameron, C. M. Kudsia, and R. R. Mansour, "Analysis of multiport microwave networks," in *Microwave Filters for Communication Systems*. Hoboken, NJ, USA: Wiley, 2018, pp. 147–175.

[20] R. J. Cameron, C. M. Kudsia, and R. R. Mansour, "Design and physical realization of coupled resonator filters," in *Microwave Filters for Communication Systems*. Hoboken, NJ, USA: Wiley, 2018, pp. 457–484.

[21] D. M. Pozar, *Microwave Engineering*. New York, NJ, USA: Wiley, 2011.

[22] M. Latif and A. U. Salfi, "General optimization algorithm for reduction of coupling matrix of chebyshev filtering functions," in *Proc. 9th Int. Bhurban Conf. Appl. Sci. Technol. (IBCAST)*, Jan. 2012, pp. 373–378.

[23] R. J. Cameron, C. M. Kudsia, and R. R. Mansour, "Waveguide realization of single-and dual-mode resonator filters," in *Microwave Filters for Communication Systems*. Hoboken, NJ, USA: Wiley, 2018, pp. 427–455.

[24] C. M. Kudsia, V. E. Boria, and S. Cogollos, "Practical Considerations and Design Examples," in *Microwave Filters for Communication Systems*. Hoboken, NJ, USA: Wiley, 2018, pp. 785–860.

[25] G. Macchiarella, G. G. Gentili, C. Tomassoni, S. Bastioli, and R. V. Snyder, "Design of waveguide filters with cascaded singlets through a synthesis-based approach," *IEEE Trans. Microw. Theory Techn.*, vol. 68, no. 6, pp. 2308–2319, Jun. 2020.

[26] M. Yu, "Power-handling capability for RF filters," *IEEE Microw. Mag.*, vol. 8, no. 5, pp. 88–97, Oct. 2007.

MUHAMMAD LATIF received the B.Sc. degree in electrical engineering from the University of Engineering and Technology (UET) Lahore, Pakistan, and the M.Sc. degree in satellite communications engineering from the University of Surrey (UniS), U.K., in 2003 and 2006, respectively. He is currently pursuing the Ph.D. degree with the Department of Electrical Engineering, UET Lahore. Since 2003, he has been working with public sector research organization, where he has participated in the design and development of microwave passive components and filters. He is also associated with the Institute of Space Technology (IST) Research Labs Lahore. His core research interests include synthesis and realization of microwave filters and multiplexing networks.

GIUSEPPE MACCHIARELLA (Fellow, IEEE) is currently a Professor of microwave engineering with the Department of Electronic, Information and Bioengineering, Politecnico di Milano, Italy. His research activity has included the past several areas of microwave engineering: microwave acoustics (SAW devices), radio wave propagation, numerical methods for electromagnetic, power amplifiers, and linearization techniques. He has been a Scientific Coordinator of PoliEri, a research laboratory on monolithic microwave integrated circuit (MMIC), which was jointly supported by Politecnico di Milano and Ericsson Company. His current activities are mainly focused on the development of new techniques for the synthesis of microwave filters and multiplexers. He authored or coauthored more than 150 papers on journals and conferences proceedings. He has been responsible of several contracts and collaborations with various companies operating in the microwave industry. He has been the Chair of IEEE Technical Committee MTT-8 (Filters and Passive Components). He is serving since several years in the TPC (Technical Program Committee) of the IEEE International Microwave Symposium and European Microwave Conference.

FAROOQ MUKHTAR received the B.Sc. degree from the University of Engineering and Technology (UET), Lahore, Pakistan, in 2007, and the M.Sc. degree in microwave engineering and the Dr.-Ing. degree under Prof. Peter Russer from Technical University Munich, Germany, in 2009 and 2014, respectively. He started his career as Tutor for high-frequency course and as Lab-Engineer for electromagnetic compatibility (EMC) testing in UET. During that time he has worked as a part-time scientific co-worker at the Institute for Nanoelectronics on algorithms for Brune's synthesis of multiport circuits and conducting tutorials on post-graduate course quantum nanoelectronics. He is currently an Assistant Professor with UET Lahore, working on high frequency topics; leaky wave and configurable antennas, filters, and metamaterials. He is also consulting Smart Wires, Inc. through Powersoft19 in the areas of electromagnetic simulations and compatibility.